Desalination and Water Treatment
www.deswater.com
doi: 10.5004/dwt.2021.27655

234 (2021) 361–375
September

Highly chlorine resistant polyamide reverse osmosis membranes realized by interfacial polymerization at a free interface with a buffer layer

Qing Zhang[a,†], Zhenping Ma[a,†], Xin Jing[a,*], Hao-Yang Mi[a,b], Yuejun Liu[a], Songwei Li[b]

[a]*Key Laboratory of Advanced Packaging Materials and Technology of Hunan Province, Hunan University of Technology, Zhuzhou 412007, China, emails: jingxin@hut.edu.cn (X. Jing), 1667402901@qq.com (Q. Zhang), 2095581941@qq.com (Z. Ma), mihaoyang@zzu.edu.cn (H.-Y. Mi), yjliu_2005@126.com (Y. Liu)*
[b]*Key Laboratory of Materials Processing and Mold, Zhengzhou University, Zhengzhou 450000, China, email: lsw626@163.com*

Received 1 March 2021; Accepted 21 July 2021

ABSTRACT

The polyamide (PA) reverse osmosis (RO) membranes prepared by interfacial polymerization at a free aqueous–organic interface always suffer from polymerization instability on the free-interface and low chlorine resistance. Focusing on these problems, in this study, a new approach was proposed which introduced an additional buffer layer to assist the free-interfacial polymerization (BLFIP). And due to the adjustment of the mitigation of the organic phase and water phase on the free-interface, defect-free PA membranes with significantly improved surface smoothness were successfully prepared by the proposed BLFIP process and the resultant membranes demonstrated superior desalination performance compared to the PA membranes prepared with the previous technique. With the optimized concentration of 0.3 wt.% trimesoyl chloride (TMC) and 0.6 wt.%, m-xylylenediamine, the prepared BLFIP PA membrane showed salt rejection rate of 92.55%, 92.01%, 83.99% and 95.16%, to Na_2SO_4, $MgSO_4$, NaCl and methyl orange, respectively at 5 bar, while maintained a water flux of about 2 Lm^{-2} h^{-1} bar^{-1}. More importantly, the BLFIP PA membrane possesses excellent long-term stability, and chlorine resistance comparing with traditional PA membranes based on TMC and m-phenylenediamine, which demonstrated the new method in this study paved a facile way for preparing RO filtration membranes with outstanding performance in seawater desalination.

Keywords: Free-interfacial polymerization; Reverse osmosis membrane; Polyamide; Buffer layer; Desalination; Chlorine resistance

1. Introduction

As a result of population growth, improved living standards, and rapid industrialization, the demand for freshwater continues to increase [1], resulting in water shortages that remain a major challenge for humanity today. Seawater desalination that includes seawater freezing, electrodialysis, distillation, membrane treatment, and ion exchange can provide usable water for our daily life and industrial processes [2]. In recent years, membrane separation technology has attracted tremendous attention on account of its advantages of high efficiency, energy-saving, and environmental protection [3–5]. The membrane separation consumes less energy in the liquid than the traditional distillation and evaporation [6,7]. For the same amount of liquid, it takes only a tenth of the energy that heat treatment requires [6]. Owing to its high-energy efficiency, reverse osmosis (RO) has become a widely applied desalination technology [8–11]. Organic polymer filter membranes have the characteristics of low-cost, facility processing, flexibility, controllable pore size and flux. The use of RO membranes for sewage treatment and seawater desalination originated

* Corresponding author.

† These authors contributed equally to this paper.
The authors declare no competing financial interest.

from asymmetric cellulose acetate membranes developed by Loeb and Sourirajan in the 1960s [12]. The second breakthrough of RO membranes was the development of high-flux thin-film composite (TFC) membranes through interfacial polymerization [13–16]. The third breakthrough of RO membranes is the ultrathin polyamide (PA) membrane with a thickness of only a few nanometers synthesized by Jiang et al. [17] by a novel interfacial polymerization process. Since the 1980s, academic and business communities have been vigorously developing high-performance RO filtration membranes, the main materials used include cellulose acetate, aromatic polyamide, polyoxadiazole, polybenzimidazole, polysulfone, etc. Although the filter membrane can achieve more than 99% salt rejection, its water flux is low, and the reverse osmosis pressure required over 50 bar during the purification process, which still leads to high energy consumption.

TFC membranes have been recognized as promising organic polymer filter membranes because of their high permeability, selectivity, chemical resistance, and low fouling tendency [18]. Thin-film composite membranes are composed of a surface layer and an underlying support layer. The surface of the filter membrane is the key to achieve reverse osmosis desalination, which was fabricated via interfacial polymerization (IP) of two monomers reacting in a biphase system (i.e., aqueous–organic phases) [19,20] and its asymmetric porous support membrane is usually macropore microfiltration (MF) or microfiltration membrane which is mainly used to provide mechanical support so that to prevent the surface layer from being damaged by the water flow or under pressure. Four prevalent techniques including IP [21–23], surface grafting [24–27], layer-by-layer self-assembly [28], biomimetic bonding, and 3D printing (different from the 3D bio-printing [29–31]) have been used for the preparation of TFCs. The IP approach is simple, mature, and the reaction condition is mild and fast. Although IP technology is relatively mature, there are still some practical and fundamental problems to be solved. The challenges are control of monomer diffusion and regulate the dynamics of the rapid polymerization that occurred at the immiscible organic-aqueous interface [32]. The nonuniform reaction on the interface would cause the accumulation and overlapping of polymer chains during the IP reaction, which leads to reduced RO membrane performance.

Polyamide (PA) TFC membrane is the most promising RO membrane for seawater desalination due to its high osmotic selectivity and good chemical stability [7,33]. Traditionally, PA TFC membranes are synthesized by two monomers (e.g., m-phenylenediamine (MPD) and trimesoyl chloride (TMC), which are dissolved in incompatible solvents. Because of their high permeability, high selectivity, excellent robustness, and durability in a broad range of pH (2–11) and temperature (0°C–45°C), PA TFC membranes have been widely utilized in many processes such as desalination, wastewater treatment, water purification, and industrial substances separation [34,35].

Nevertheless, PA TFC membranes also face many problems that greatly limit their broader applications, such as chlorination degradation, biological pollution, organic pollution, etc. Among them, chlorination degradation is urgently needed to be solved. In the process of water treatment, the feedwater often contains a large number of biological pollutants, which requires the use of Cl_2 as a disinfectant to be added to the water. This often results in active chlorine molecules in the water. Once the active chlorine molecules come into contact with the polyamide composite membranes, the active chlorine molecules would destroy the PA separation layer which degrades the composite membranes, leading to a sharp decline in the performance of the membranes [36]. This will inevitably lead to the increase of membrane replacement frequency, the reduction of separation efficiency, and the increase of production and operation costs. Therefore, the development of a chlorine-resistant polyamide composite membrane is an urgent demand to solve these problems.

In recent years, efforts have been made to improve the chlorine resistance of PA TFC membrane [37]. Shi et al. [38] combined polyamide with graphite oxide to produce a composite membrane with improved chlorine resistance. Lu et al. [28] prepared the chlorine-resistant composite membrane by the layered double hydroxide-modified method. Lin et al. [39] prepared PA composite membranes with excellent chlorine resistance via surface modification. Hu et al. [40] prepared high-producing chlorine-resistant membrane via IP method by using a novel amine monomer 2,2'-bis(1-hydroxyl-1-trifluoromethyl-2,2,2-trifluoroethyl)-4,4'-methylenedianiline (BHTTM). Zhang et al. [41] prepared a chlorine-resistant membrane by IP method using piperazine (PIP) and BHTTM as water phase monomers and TMC as organic phase monomers. Using m-xylylenediamine (m-XDA) and polyethyleneimine (PEI) as water monomers, Liu et al. [42] prepared a water treatment membrane with high chlorine resistance through the IP process. The m-XDA has a methylene group between the amine group and the benzene ring, which not only reduces the activity of the amide bond but also increases the steric hindrance and reduces the possibility of Orton rearrangement to improve membranes chlorine resistance [43]. Therefore, m-XDA could be a promising candidate monomer for developing novel chlorine-resistant PA RO membranes.

In this study, aiming at the aforementioned two grand challenges, a buffer layer was introduced in the aqueous-organic interface to regulate the diffusion of monomers and realize the precise control of the reaction rate. Moreover, m-XDA was used as the organic phase in the BLFIP process intended to improve the chlorine resistance of the synthesized PA membrane. Commercial nylon 66 MF membranes with high mechanical strength, hydrophilic, toughness, and elasticity were chosen as the support layer to fabricate the TFC RO membranes using the BLFIP process. The effects of m-XDA, TMC concentration ratio, and reaction time on the holistic performance of PA TFC membrane were studied comprehensively. The optimized PA RO membrane exhibited high salt rejection to various salts including methyl orange, $MgSO_4$, Na_2SO_4, and NaCl. Excellent chlorine resistance of the developed PA RO membrane was verified by reactive chlorine (1,000 ppm) treatment for 12 h demonstrating promising long-term stability and practical applicability in chlorine-rich circumstances.

2. Experimental

2.1. Materials

PA66 microfiltration organic filter membrane with a pore size of 0.22 μm was purchased from Shaoxing Shangyu Aike Instrument Equipment Co., Ltd., (China). m-xylylenediamine (m-XDA, 99%), anhydrous sodium sulfate (Na_2SO_4, ≥99.0%), anhydrous magnesium sulfate ($MgSO_4$, AR, 99.5%), sodium chloride (NaCl, AR, 99.5%), trimesoyl chloride (TMC, 265.48 MW), n-hexane (AR, 97%) were purchased from Shanghai Aladdin Reagents Company, (China). Sodium hydroxide (NaOH, AR) and sodium hypochlorite solution (NaClO, AR, active chlorine content 10%) were purchased from McLean (Mcklin reagent Company, China). Methyl orange was purchased from Tianjin Tianxin Fine Chemical Development Center, (China). Concentrated hydrochloric acid (HCl, GR) was purchased from Zhuzhou Xingxing Glass Co. Ltd., (China). Anhydrous ethanol was purchased from Sinopac Chemical Reagent Co., Ltd., China. Deionized (DI) water was provided by Milli-Q.

2.2. Membrane preparation

The support layer of PA66 with a diameter of 50 mm and average pore size of 0.22 μm was immersed in anhydrous ethanol for 60 s at room temperature, followed by ultrasonication in deionized water for 150 s to remove impurities and particles trapped in the membrane. Cleaned membranes are stored in deionized water until use. Defined amount of m-XDA and TMC were dissolved in deionized water and hexane, respectively, to prepare aqueous and organic solution with different concentrations (e.g., 0.3 wt.% m-XDA-0.15 wt.% TMC, 0.4 wt.% m-XDA-0.2 wt.% TMC, 0.5 wt.% m-XDA-0.25 wt.% TMC, 0.6 wt.% m-XDA-0.3 wt.% TMC, 0.7 wt.% m-XDA-0.35 wt.% TMC). The PA RO membranes prepared using different concentrations of m-XDA and TMC solution were named as BLFIP1, BLFIP2, BLFIP3, BLFIP4 and BLFIP5, respectively, as the increase of overall monomer concentration in the solvents. Support layers were placed at the bottom of the glass reactor with a diameter of 60 mm followed by pouring 20 mL m-XDA solution. n-hexane was added onto the surface of the aqueous phase to form a buffer layer with a thickness of 3.5 mm. Then, 5 mL TMC solution was slowly added to the buffer layer along the wall of the reactor. The reactor was sealed using parafilm and stored at 25°C for 20 min to allow complete reaction on the interface. The PA membrane formed was taken out using the support membrane carefully to ensure that the membrane was tiled on the surface of the PA supporting membrane without cracks. The PA TFC membrane prepared by BLFIP was cleaned with n-hexane and deionized water respectively and dried for 12 h before use. Meanwhile, BLFIP-FI membranes based on 0.6 wt.% m-XDA-0.1 wt.% TMC and 0.6 wt.% m-XDA-0.15 wt.% TMC were prepared by the BLFIP method, which was named as BLFIP-FI1 and BLFIP-FI2 films, respectively.

The composite membranes based on MPD/TMC were prepared by the BLFIP process using 0.6 wt.% MPD solution and 0.3 wt.% TMC solution, which was named as BLFIP-MPD membrane.

PA TFC membranes were prepared by conventional free interface-interfacial polymerization (FI-IP) process without the buffer layer for comparison. In addition, a traditionally used PA TFC membrane was synthesized using TMC (0.3 wt.%) and MPD (0.1 wt.%) by the FI-IP process for comparison and evaluation of the monomer effect.

2.3. Characterization

The chemical structure of BLFIP membranes was studied by the Fourier transform infrared spectrometer (FTIR, Nicolet 380, USA) at a measurement frequency ranged from 4,000–400cm^{-1}. The surface elemental composition of BLFIP membranes was analyzed using X-ray photoelectron spectroscopy (XPS, Thermo Fisher, ESCALAB Xi$^+$, USA) with Al-K radiation as an X-ray source. The working voltage used was 12.5 kV and the filament current was 16 mA. The survey scan and high-resolution C1s core level scan were performed.

The surface morphology of BLFIP membranes and supporting PA layer was characterized by a scanning electron microscope (SEM, Tescan Mira3, Czech). To reduce the charging effect, an ultrathin gold layer was coated on samples before imaging at 10 kV. The surface topography of BLFIP membranes was characterized by atomic force microscopy (AFM, Bruker Dimension ICON, USA) in a tapping mode. For the AFM sample preparation, the BLFIP membrane was collected from the interface using a silicon wafer as the support (Fig. S2b, obtaining independent PA layer).

The water contact angle (WCA) was measured using a contact angle measuring instrument (CA100B, China) to evaluate the hydrophilicity of the membrane surface. Approximately 5 μL deionized water was dropped onto the membrane surface using a microsyringe. The WCA value was measured after the water droplet stayed on the membrane surface for 30 s. Each WCA value was obtained by using more than five different locations on each membrane.

2.4. Membrane performance evaluation

The desalination performance of the prepared membranes was evaluated by a separation membrane instrument (HP4750 Stirred Cell, Sterlitech, USA) with an effective area of 14.6 cm^2. Process flow chart of the desalting test (Fig. S3). The experiment was carried out with a feed pressure of 5 bar against NaCl, Na_2SO_4, $MgSO_4$, and methyl orange (HIn) solutions with a concentration of 2.0 g L^{-1} at ambient temperature. The membranes were pre-pressurized with DI water for 1 h to reduce the effect of concentration polarization before the desalination test. The feed solution was stirred by magnetic stirring equipment (ZGCJ-3A, China). After running stably, performance data were measured. The water flux (F) in the unit of Lm^{-2} h^{-1} bar^{-1} and the salt rejection rate (R) in the unit of % were calculated according to the following equations:

$$F = \frac{V}{At\Delta P} \tag{1}$$

$$R = \left(1 - \frac{C_p}{C_f}\right) \times 100\% \tag{2}$$

where V is the permeate volume, t is the permeate time, and ΔP is the feed pressure; C_f is the salt concentration of the feed solution, and C_p is the salt concentration of permeate solution which were measured by a conductivity meter (Mettler Toledo F3-Standard, China).

2.5. Treatment of BLFIP PA membranes with a chlorine solution

Active chlorine is inevitable in the raw solution of seawater desalination or water treatment. Active chlorine solution was prepared by 1,000 ppm sodium hypochlorite solution with pH adjusted to 7.0 using standard HCl and NaOH solutions. Test membranes were immersed in the active chlorine solution for up to 12 h. The concentration (ppm) and the treatment time (h) were used as the index for the treatment intensity of active chlorine [44]. To prevent the degradation of active chlorine, the experiments were carried out and kept in the dark. The treated membranes were further immersed in DI water for 1 h and rinsed and dried before testing.

2.6. Statistical analysis

One-way ANOVA analysis was performed to determine the statistical significance of the measured results. We used Tukey's multiple comparison tests ($p \leq 0.05$, 0.01) to determine whether a significant difference existed between different groups for the same property.

3. Results and discussion

3.1. Surface chemical composition of BLFIP PA membranes

Different from the typical FI-IP process, the BLFIP process developed in this study introduces a buffer layer between the organic phase and water phase, which could prevent the fluctuation on the interface when adding the organic phase into the water phase and improve the uniformity of reactive monomers (TMC) in the organic phase by increasing diffusing time of monomers in the buffer layer as depicted in Fig. 1a and b. The reaction rate on the free interface is thus decreased which is favorable for the formation of a more homogenous and defect-free membrane (Fig. 1c). The obtained PA membrane on the free interface is then carefully transferred onto a support layer and rinsed with excess hexane to remove residue TMC and water.

The surface of BLFIP membranes was characterized by FTIR and XPS to investigated the chemical composition of the synthesized PA membranes. The peaks that appeared at 1,647 and 1,535 cm^{-1} on the FTIR spectra (Fig. 2) corresponded to the characteristic peaks of the amide II (N–H) band and the amide I (C=O) band of the amide group (–CO–NH–), respectively [42]. For the BLFIP membranes synthesized at different monomer concentration, it is clear that the amide composition was enhanced as the increase of monomer concentration because of the gradually increased relative concentration of m-XDA. The FTIR results verified the successful synthesis of PA membranes.

XPS was used to quantitatively analyze the chemical composition at 1–5 nm depth on the surface. C, N, and O elements were detected on the surface of BLFIP membranes (Fig. 3). As shown in Table 1, the atom percentage of C, N, and O was about the same for BLFIP membranes. The content of N increased with the enlargements of reactant concentration, while the content of C decreased significantly with the decrease of reactant concentration. This implies that the increase of the reactant concentration resulted in the improvement of the amide content of the BLFIP membranes.

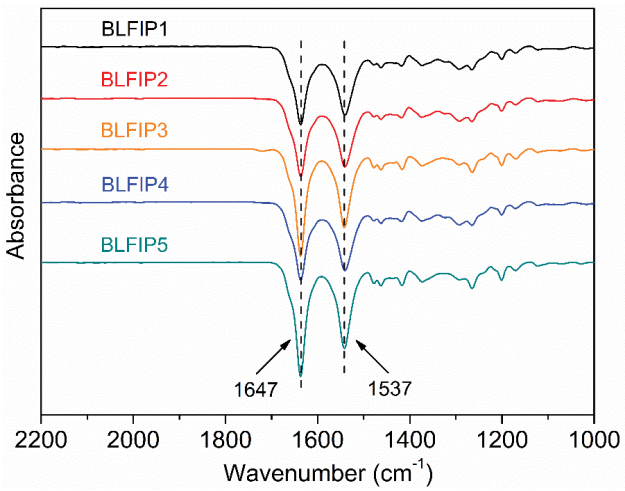

Fig. 2. FTIR of BLFIP membranes.

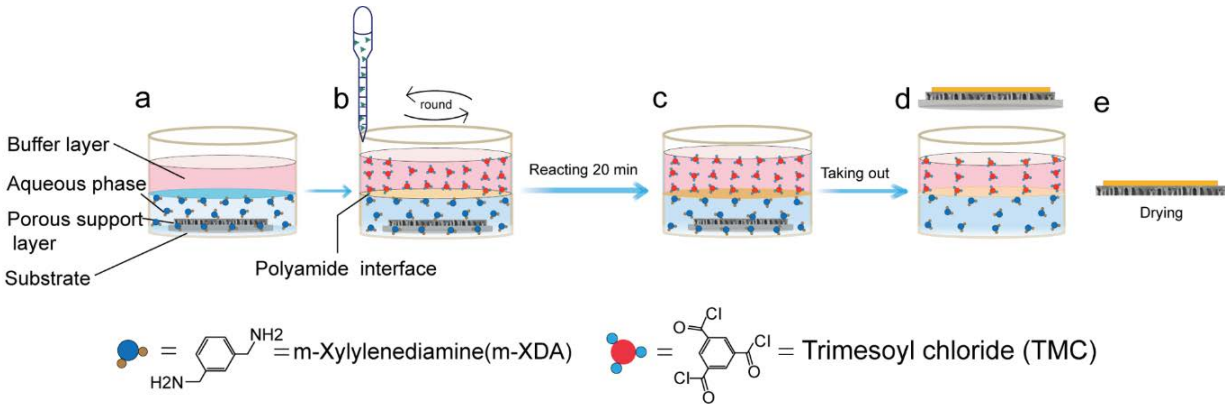

Fig. 1. Schematic illustration of the BLFIP process to prepare PA TFC membranes.

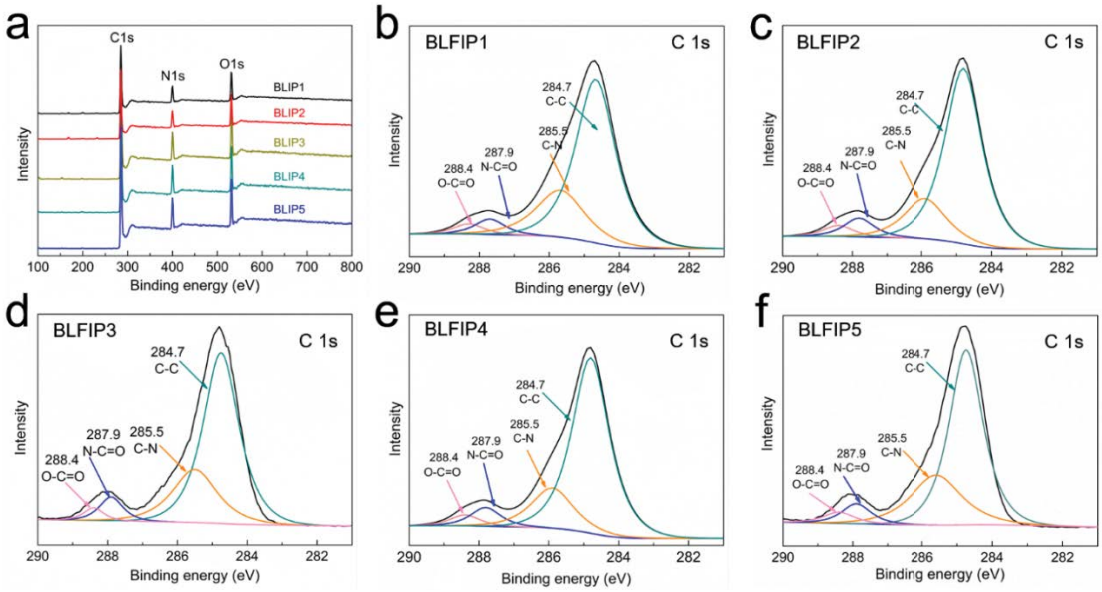

Fig. 3. XPS spectra and C1s core level spectra resolving results of BLFIP membranes.

Table 1
Surface atomic composition analysis of BLFIP membranes

Sample	Surface atomic composition			
	C (%)	N (%)	O (%)	O/N
BLFIP1	75.64	11.09	13.27	1.20
BLFIP2	75.52	11.32	13.16	1.16
BLFIP3	75.35	11.64	13.01	1.12
BLFIP4	75.13	11.83	13.04	1.10
BLFIP5	75.04	11.93	13.03	1.09

O/N atomic ratios have been used to estimate the degree of cross-linking of surface PA layers [45] and explore the influence of concentration on the formation of surface PA layer by interfacial polymerization. Theoretically, the O/N atomic ratio of all linear PA is 2, and the O/N atomic ratio of all cross-linked PA is 1 [46]. From the O/N atomic ratio of BLFIP membranes in Table 1, it can be seen that the O/N ratio decreases as the increase of monomer concentration indicating the cross-linking degree of PA was gradually increased, which would result in a denser PA surface layer. The C1s core energy level spectrum of BLFIP membrane showed four peaks (Fig. 3b–f) in 284.7 eV (C–C, C–H), 285.5 eV (C–N), 287.9 eV (N–C=O), and 288.4 eV (O–C=O), confirming the existence of amide and carboxyl groups [37]. The percentage for the chemical bonds of the peak split of C1s measured from the surface of the BLFIP membranes was showed in Table S1, which was consistent with the results of Table 1. The XPS and FTIR spectra confirmed that the surface PA layer which plays the role of desalination was successfully formed during the BLFIP process.

3.2. Surface morphology of BLFIP PA membranes

Fig. 4 shows SEM images of support layer (Fig. S1), FI-IP PA membranes (Figs. 4a, c, e, and S1c), and BLFIP PA membranes (Figs. 4b, d, f, and S1d). The rear surface of the support layer (Fig. S1b) is relatively flat and has a smaller pore size compared with the front surface (Fig. S1a), which should be more desirable for the protection of the surface layer from cracking or being crushed during desalination under pressure. Therefore, the rear surface of the PA support layer was used to receive the BLFIP membranes. As shown in Fig. 4a, c, e, as the increase of m-XDA and TMC monomer concentrations in the aqueous and organic solutions, increasing aggregated particles and folds were observed on the surface of FI-IP membranes. The agglomerations on the FI-IP membrane surface were likely because of the rapid and nonuniform reaction of TMC with m-XDA on the free interface since the region where TMC solution was added would have a greater concentration than other regions. During the whole polymerization process, TMC molecules tend to pile and polymerize with m-XDA in the location where they are added which led to the formation of aggregates and folds, and the nonuniformity of the whole PA membrane. On the contrary, as shown in Fig. 4b, d, f, the surfaces of PA membranes prepared using the BLFIP technique displayed smoother and more uniform morphology compared with the PA membranes prepared using the FI-IP method. As the increase of m-XDA and TMC monomer concentration in aqueous solution and organic solution, the initial change of surface morphology was not very obvious until the concentrations reached 0.7–0.35 wt.% for m-XDA and TMC monomers at which micro folds were observed on the membrane surface. These results indicated that the incorporation of a buffer layer in the free-interfacial polymerization process is highly favorable for the formation of uniform and homogenous PA membranes, which may be ascribed to the following reasons: firstly, the buffer layer facilitated the diffusion of TMC monomers by giving more time for the TMC monomers to reach the oil-water interface; Second, the concentration of TMC was slightly diluted in the hexane phase by the buffer layer

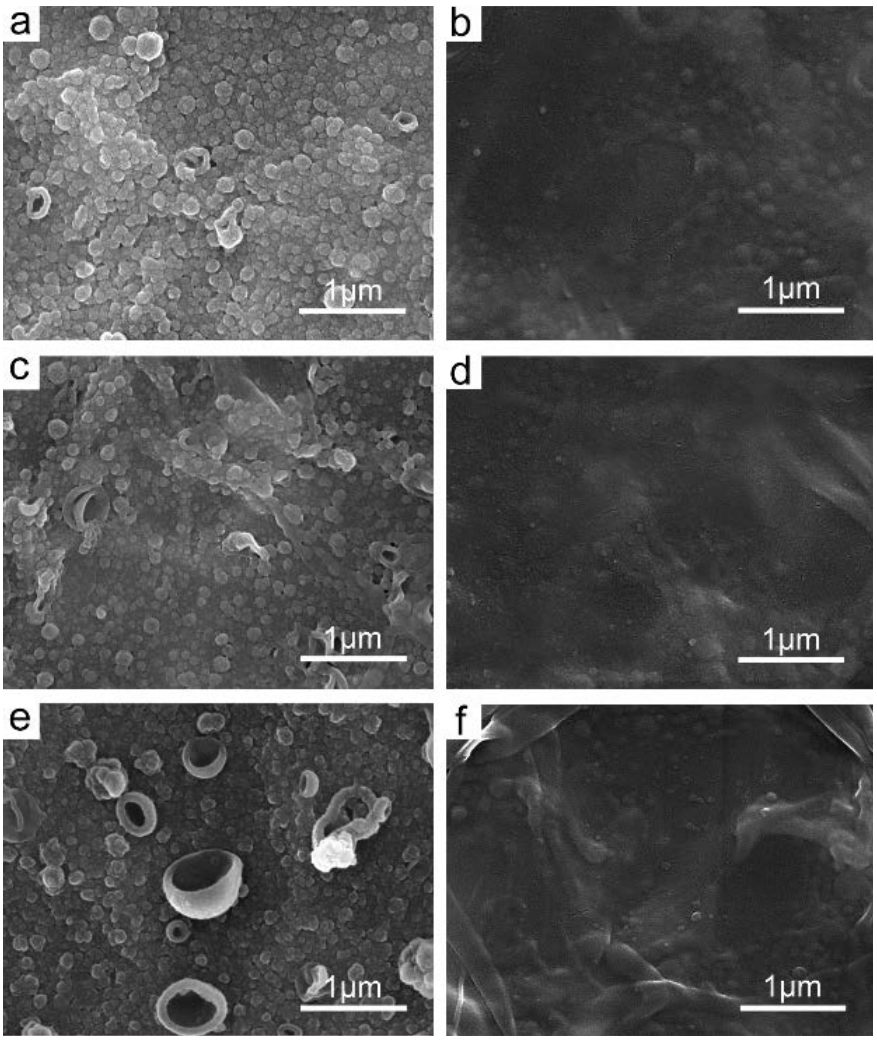

Fig. 4. SEM images of (a, c, e) FI-IP membranes prepared with m-XDA and TMC concentrations of 0.3–0.15 wt.%, 0.5–0.25 wt.%, 0.6–0.3 wt.%, and 0.7–0.35 wt.%, respectively; SEM images of (b, d, f) BLFIP3, BLFIP4, and BLFIP5 membranes.

which effectively reduced the reaction rate on the interface, and it could prevent the formation of over polymerized aggregates and micro folds.

AFM measurements were carried out to investigate the morphology and the roughness (R_a) of BLFIP and FI-IP membranes as shown in Fig. 5 and Table 2. The surface roughness of BLFIP membranes gradually increased as the concentrations of m-XDA and TMC was increased. Similarly, the surface roughness of BLFIP1, BLFIP3, and BLFIP4 were 24.1, 42.7, and 62.4 nm, respectively. However, When the ratios of m-XDA and TMC were 0.7 and 0.35 wt.%, the surface roughness of the BLFIP5 membrane increased sharply to 147 nm, whose result was consistent with the results of the SEM image of BLFIP membranes. This was because when the concentration of reactants was too high, the buffer layer could play a limited role in the uniform dispersion of TMC, leading to rapid and violent polymerization reaction between m-XDA and TMC at the local interface of the aqueous–organic interface, resulting in irregular accumulation and folding of the surface PA layer. Similarly, it could be seen that the surface roughness of FI-IP films also increased with the increase of reactant concentration from 89.5 to 186 nm. It was worth noting that the surface roughness of FI-IP films was greater than that of BLFIP membranes since the fast polymerization in the FI-IP process was more rapid which is favorable for the formation of a rough surface. The AFM results are consistent with the trends revealed in the SEM images, which further demonstrated that the introduction of the buffer layer is beneficial for the formation of a smooth PA membrane through interfacial polymerization.

3.3. Surface hydrophilicity of BLFIP PA membranes

Membrane surface hydrophilicity is an essential factor to determine the flux and antifouling performance of RO membranes [47]. WCA is the main method to characterize the wettability of a material surface. Materials with good hydrophilicity generally have a lower contact angle, and vice versa. The more hydrophilic the membrane surface is, the more favorable it is for water molecules to pass through the composite membrane [48]. The changes of WCA

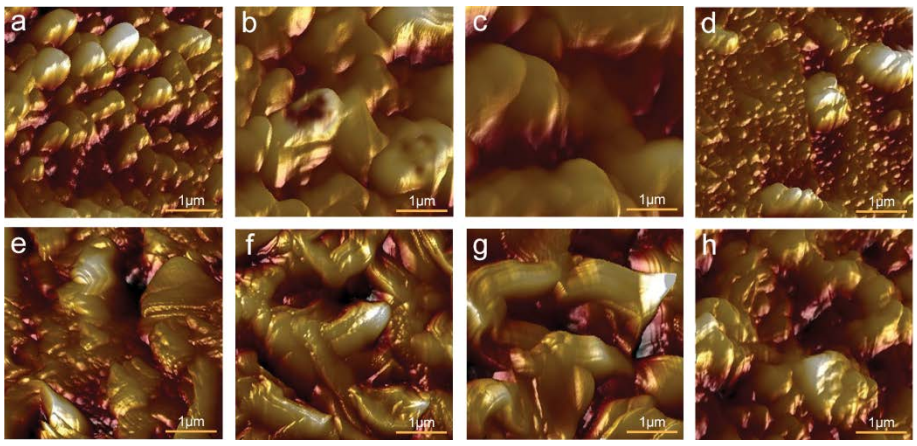

Fig. 5. AFM height images of the BLFIP and FI-IP membranes (a) BLFIP1, (b) BLFIP3, (c) BLFIP4, (d) BLFIP5, (e) FI-IP1, (f) FI-IP3, (g) FI-IP4, and (h) FI-IP5 membranes.

Table 2
The surface roughness (R_a) of BLFIP and FI-IP membranes

Membrane	BLFIP1	BLFIP3	BLFIP4	BLFIP5
R_a (nm)	24.1	42.7	62.4	147
Membrane	FI-IP1	FI-IP3	FI-IP4	FI-IP5
R_a (nm)	89.5	96.7	136	186

of BLFIP membrane surface with time are shown in Fig. 6. The WCAs of BLFIP3 and BLFIP5 were below 90° and were decreased rapidly in a short time. It was observed in the experiment that the water droplets were gradually permeated through the BLFIP membranes over time rather than spread across the membrane surface indicated by the gradual decrease of droplet volume. This phenomenon not only implies the excellent hydrophilicity of the membrane surface but also suggests that the membrane allows the penetration of water molecules. With the increase of monomer concentration from 0.5–0.25 wt.% to 0.7–0.35 wt.%, the initial WCA decreased from 50.3° to 44.9°, and the WCA changed to 22.6° and 11.4° at after 60 s, respectively. The membrane hydrophilicity is related to the surface properties including chemical composition and roughness [42]. It can be concluded that the increase of hydrophilicity was mainly attributed to the increase of the hydrophilic amid bonds on the membrane surface as the monomer concentration was increased since the roughness was increase simultaneously.

3.4. BLFIP membrane performance evaluation

The salt rejection performance test results of developed BLFIP membranes are shown in Fig. 7. The rejection rate and water flux of BLFIP membranes maintained the same trend to various salts. It was found that the rejection rate was increased while the water flux decreased with the increase of monomer concentration, and the optimum rejection performance was achieved by the BLFIP4 membrane (i.e., 0.6 wt.% m-XDA and 0.3 wt.% TMC). The statistical significance analysis indicated that the difference in salt rejection rate and water flux was statistically significant

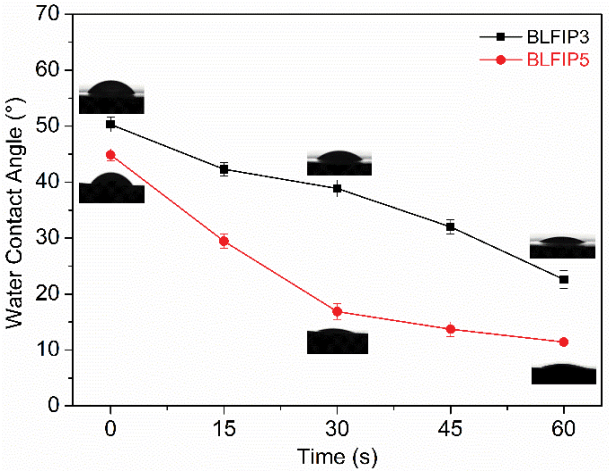

Fig. 6. Change of water contact angle on BLFIP3 and BLFIP5 membrane surfaces in 60.

among membranes fabricated using different formulas. In addition, further increase of monomer concentration led to the simultaneous reduction of rejection rate and water flux. At low monomer concentration, the increase of the rejection rate may be because the membrane became thicker and denser as the increases of reactants concentration, which led to greater salt retention. At high monomer concentration, as indicated by the SEM images, irregular accumulation and folding in some regions of the membrane start to form, which led to nonuniformity of the whole membrane and potential defects in some areas. The continuous decrease of water flux was because the increased membrane thickness greatly hindered the penetration of water molecules.

The salt rejection sequence of the optimum BLFIP4 membrane was methyl orange (95.16%) > Na_2SO_4 > (92.55%) > $MgSO_4$ (92.01%) > NaCl (83.99%), and the water flux of the BLFIP4 membrane maintained about 1.9 Lm^{-2} h^{-1} bar^{-1} to various salts. It is worth mentioning that salt rejection of BLFIP4 for NaCl was much higher than recent studies by Ma et al. [49] (<20%) and Peng et al. [50] (<30%). Meanwhile, we compared the performance of BLFIP membrane with

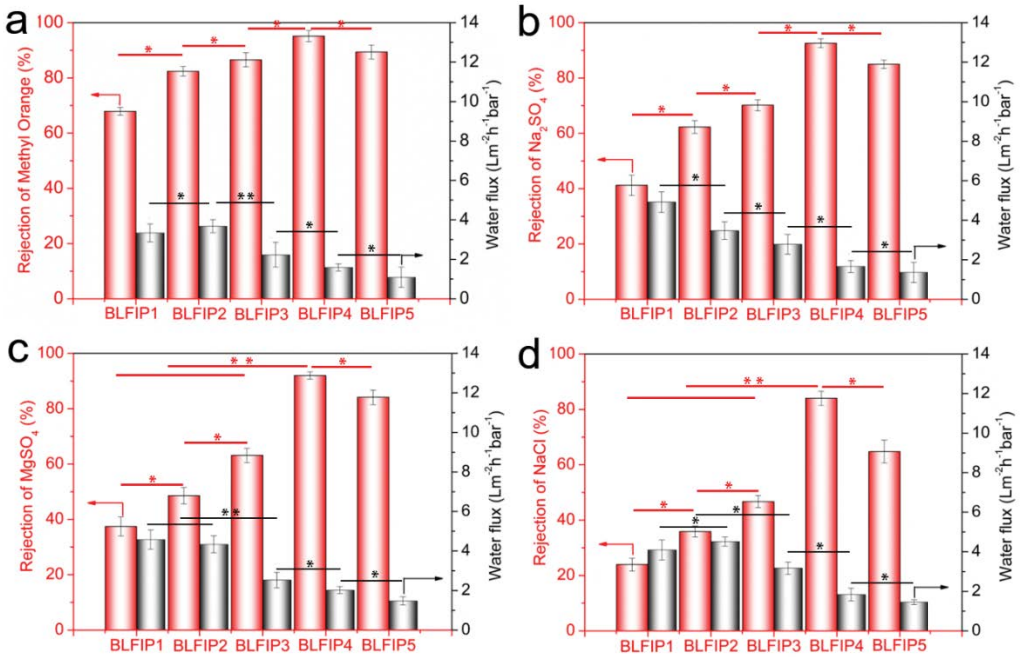

Fig. 7. The salt rejection and water flux of BLFIP membranes prepared using different monomer concentrations to various salts (a) methyl orange, (b) Na_2SO_4, (c) $MgSO_4$, and (d) NaCl.

other RO membranes reported in the literature (Table S2), and it was found that the salt rejection of BLFIP membrane for NaCl was significantly higher than the reported similar RO membranes. When compared with conventional PA membranes on m-XDA/TMC fabricated through the IP process (Table S3), it was found that the rejection rate of Na_2SO_4 was close, while the rejection of $MgSO_4$ and NaCl of the developed BLFIP membrane was much higher than the conventional IP membrane.

The main factors affecting membrane ion repulsion were the steric hindrance and the Donnan effect, and the salt rejection could be explained by the synergistic effect of pore sieve and Donnan repulsion [51]. The front surface of BLFIP membranes was in contact with the organic phase, after the reaction, the carboxyl groups were mostly concentrated in the organic phase, while the amino groups were mostly concentrated on the rear surface in contact with the water phase [17]. The highest rejection of methyl orange was attributed to its largest molecular weight of 327.34 g mol^{-1} which was subjected to a great steric hindrance effect, and the repulsive effect on the membrane surface to the $C_{14}H_{14}N_3O_3S^-$ ions. The distinct greater desalination rate of Na_2SO_4 and $MgSO_4$ than NaCl was mainly attributed to the synergetic effect of steric hindrance, electrostatic repulsion, and Donnan repulsion. Mg^{2+} has a larger radius than Na^+, and the hydration ion radius of SO_4^{2-} is larger than Cl^-. Moreover, the PA membrane showed weak repulsion against monovalent cations (e.g., Na^+) or polyvalent cations (e.g., Mg^{2+}), but strong repulsion against anions (e.g., Cl^-), especially polyvalent anions (e.g., SO_4^{2-}). Specifically, the repulsion to Mg^{2+} and SO_4^{2-} ions should be stronger than Na^+ and Cl^- ions since Donnan repulsion has a more obvious influence on multivalent ion repulsion [42]. Therefore, the desalination rates of Na_2SO_4 and $MgSO_4$ were greater than NaCl. Comparing the performance in $MgSO_4$ and Na_2SO_4 salt rejection, multivalent cations (e.g., Mg^{2+}) are prone to shelter the negative charge of BLFIP membranes according to the Donnan effect, thus reducing the electrostatic repulsion, that is, screening effect [52], which resulted in the lower rejection of $MgSO_4$ than that of Na_2SO_4 of the PA membrane.

To emphasize the effect of buffer layer introduction on the desalinization performance, the salt rejection of PA membranes prepared using FI-IP and BLFIP was compared. As shown in Fig. 8, the PA membrane prepared without buffer layer (Fig. 8a) showed a much lower rejection rate to various salts compared with the PA membrane prepared with the buffer layer (Fig. 8b), although it had a slightly higher water flux. For instance, the rejection rate to methyl orange was 95.16% for the BLFIP PA membrane, while it was only 87.56% for the FI-IP PA membrane. In the case of rejecting small salt ions, the FI-IP PA membrane showed significantly inferior performance. The Na_2SO_4 rejection rate of the BLFIP PA membrane reached 92.55%, but it was only 70.50% for the FI-IP PA membrane. The remarkable improvement for the case involving the buffer layer was mainly attributed to the morphological difference between them since they share the same chemical composition. These results further testified that the smooth and uniform PA membrane obtained with the involvement of a buffer layer is highly favorable in improving the desalinization performance of the PA membranes. In addition, membranes prepared using diluted TMC solutions were compared to emphasize the effect of the buffer layer. It was found that simply reducing the concentration of TMC would result in a non-uniform reaction on the interface, defected membrane and lead to a very low salt rejection rate (less than 50%) (Fig. S4).

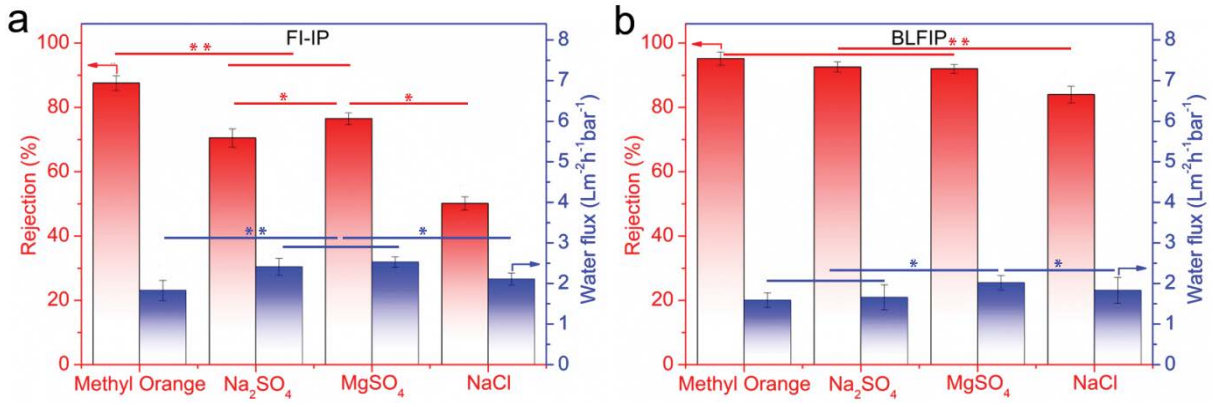

Fig. 8. The salt rejection and water flux of (a) FI-IP and (b) BLFIP for various salts.

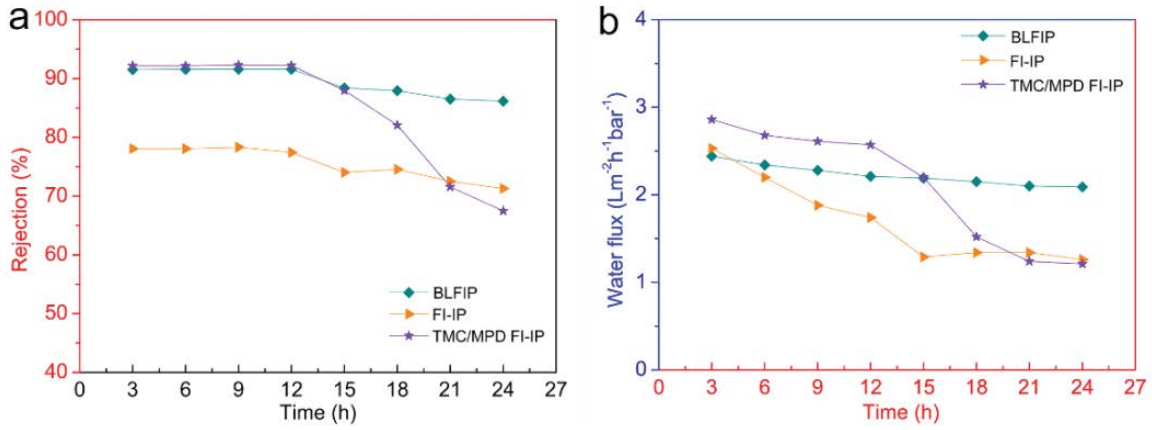

Fig. 9. Na_2SO_4 rejection and water flux change of different PA membranes prepared based on TMC/m-XDA using BLFIP and FI-IP method, and PA membrane prepared based on TMC/MPD using FI-IP method in continuous operation for 24 h.

PA TFC membranes prepared using different monomers and techniques were measured in the long-run to evaluate their continuous operation stability. From Fig. 10a, it was found that the salt rejection of the TMC/MPD based FI-IP membrane had a comparable salt rejection rate with the BLFIP membrane which was much higher than that of the FI-IP membrane prepared based on TMC and m-XDA. And the initial water flux of TMC/MPD FI-IP membrane was even higher than the BLFIP membrane (Fig. 10b). Noticeably, the salt rejection rate underwent a gradual increase and then decrease over time for all membranes. A steep reduction of water flux was also noticed for the TMC/MPD FI-IP membrane in long-run. These results indicated that the traditional TMC and MPD based PA membrane had inferior long-term stability than the PA membranes based on TMC and m-XDA. We believed that this was mainly attributed to the stiffer molecular structure of the TMC/MPD FI-IP membrane which might be easier to be clogged by the concentrated ions under pressure, which lead to the decrease of water flux in the long-term. Moreover, in our static measurement, the salt concentration would gradually increase over time, thus the rejection rate was significant reduced after 15 h implying inferior salt rejection to concentrated solutions. On the contrary, the TMC and m-XDA based PA membrane presented relatively stable performance in

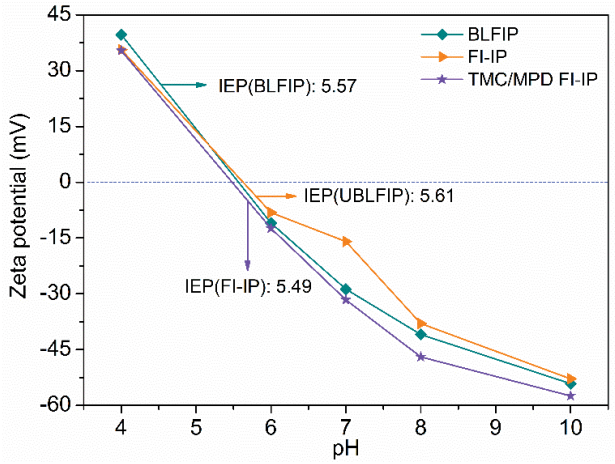

Fig. 10. Zeta potential of BLFIP, FI-IP membranes prepared based on TMC/m-XDA using respectively BLFIP and FI-IP method, and TMC/MPD FI-IP membrane prepared based on TMC/MPD using FI-IP method.

continuous operation. The BLFIP membrane maintained a high Na_2SO_4 rejection rate over 87.5% and a water flux over 2.0 $Lm^{-2}\,h^{-1}\,bar^{-1}$ even after running for 24 h. This was

because the m-XDA molecule provides additional degree of freedom to the PA molecular structure so that the membrane is more difficult to be clogged or damaged by the ions compared with the TMC and MPD based PA membrane, which resulted in the superior stability and robustness of the BLFIP membrane in long-term desalinization.

The surface potential of different PA membranes was analyzed by zeta potential. As shown in Fig. 10, three membranes showed a similar decreasing trend in zeta potential as the increase of pH levels. The iso-electric points (IEPs) of BLFIP membrane, FI-IP membrane, and TMC/MPD FI-IP membrane were 5.57, 5.61, and 5.49 respectively. The small difference in zeta potential suggested that the use of MPD or m-XDA, and the different fabrication methods had limited effects on the surface potential of PA membranes. The results indicated that all three membranes had a relatively large pH range (over 5.65) for the membrane surface to maintain negative potential, which was beneficial for the electrostatic repulsion of negatively charged ions or negatively charged groups. It was also an important reason for the higher rejection rate of Na_2SO_4 than that of NaCl for the BLFIP membranes.

To further evaluate the chlorine resistance of the developed BLFIP membrane in comparison with BLFIP-MPD membrane based on TMC and MPD, they were immersed in NaClO solution with an active chlorine concentration of 1,000 ppm for 12 h, and the product of the concentration of active chlorine and the treatment time was used to represent the treatment intensity of active chlorine (12,000 ppm h). The salt rejection rates and water flux to $MgSO_4$, Na_2SO_4, and NaCl solutions were measured and normalized by the performance of corresponding membranes prior to chlorine resistance tests. Remarkably, the salt rejection of BLFIP-MPD membrane for $MgSO_4$, Na_2SO_4, and NaCl (Fig. 11a) was all dramatically reduced to about 20% of its original level, and the normalized salt rejection was Na_2SO_4 > (16.92%) > $MgSO_4$ (16.14%) > NaCl (14.35%). While the water flux was greatly improved by over 3600% of its original level, which indicated that the molecular structure of the BLFIP-MPD membrane has been degraded by the active chlorine during the experiment. On the contrary, the BLFIP membrane (Figs. 11b and S5) showed a relatively small reduction (within 16%) in the rejection rate to various salts, and the water flux was decreased to about 45% of its original level. Meanwhile, comparing the chlorine resistance of BLFIP4 membrane (Fig. 11b) with BLFIP3 membrane (Fig. S5), when the concentration of m-XDA and TMC monomer changed, the chlorine resistance of the two was not much different. These results indicated that the main factor affecting the chlorine-resistance of the BLFIP membrane was not the concentration of m-XDA and TMC, but the difference of chlorine-resistance between them in diamine was not significant. These results indicated that the main factor affecting the chlorine resistance of BLFIP membrane was not the concentration of m-XDA and TMC, but the activity of amino in diamine.

The minor effect of active chlorine on the BLFIP membrane could be mainly attributed to the molecular structure of TMC and m-XDA based BLFIP membrane. The amide bond of the PA membrane would be attacked by the active chlorine, thus leading to the cleavage of PA molecules and the deterioration of the salt rejection capability [53]. The chlorination process of the aromatic PA membrane can be divided into two stages: the first stage is the N-chlorination of the amide bond, and the second stage is ring chlorination through Orton-rearrangement [47]. The reaction mechanism diagrams are shown in Fig. 12a and b. The methylene bond between the amine group and benzene ring in m-XDA molecule reduces the activity of amide bond, increases the steric hindrance which reduces the possibility of Orton rearrangement, and, thus improves the chlorine resistance of the TMC and m-XDA based PA membrane in comparison with conventional TMC and MPD based PA membrane [43].

4. Conclusions

In summary, a novel interfacial polymerization at a free interface method involving a buffer layer between the aqueous phase and the organic phase was developed in this study for the fabrication of high-performance chlorine resistant reverse osmosis PA membranes based on TMC and m-XDA. The introduction of the buffer layer resulted in smoother surface morphology by decreasing the polymerization rate, enhancing the dispersion uniformity of the TMC monomer, and reducing the defects of BLFIP membranes. The resulted BLFIP PA membranes with optimized monomer concentrations (0.6 wt.% m-XDA and 0.3 wt.% TMC) displayed the best desalination performance with a salt rejection to methyl orange, Na_2SO_4, $MgSO_4$, and NaCl. Compared with conventional FI-IP PA membranes based on TMC and MPD, the developed BLFIP PA membrane

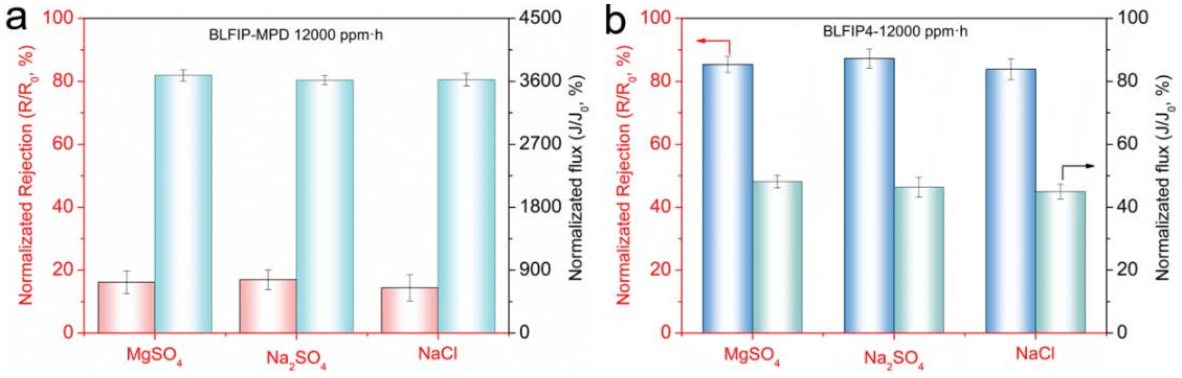

Fig. 11. Chlorine-resistant performance of (a) BLFIP-MPD and (b) BLFIP membrane.

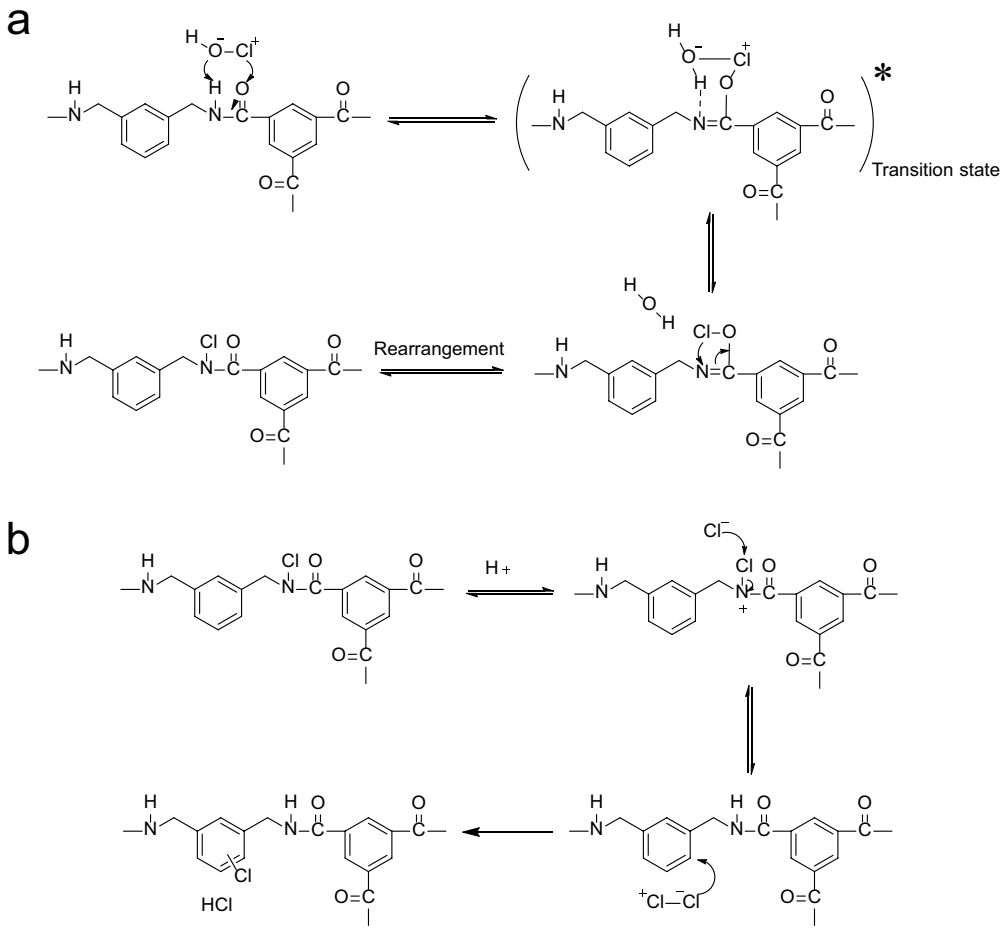

Fig. 12. Schematic illustration of (a) N-chlorination reaction mechanism of amide bond and (b) cyclo chlorination reaction mechanism of Orton rearrangement.

showed superior stability in long-term testing period due to the increased molecular chain mobility of the BLFIP PA membrane. Moreover, it also possessed outstanding performance for active chlorine resistance, owing to the decreased amide activity by the methylene bond. Therefore, the method proposed and the BLFIP PA membrane developed are highly favorable for the development of high-performance and chlorine-resistant RO membranes, which provides a new approach for the interfacial polymerization technique.

Acknowledgment

The authors would like to acknowledge the financial support from the Research Project of the Educational Commission of Hunan Province (Grant No. 18B297) and thank Xiaobin Zhou from Shiyanjia Lab (www.shiyanjia.com) for the SEM and XPS analysis.

References

[1] D.L. Zhao, S. Japip, Y. Zhang, M. Weber, C. Maletzko, T.-S. Chung, Emerging thin-film nanocomposite (TFN) membranes for reverse osmosis: a review, Water Res., 173 (2020) 115557, doi: 10.1016/j.watres.2020.115557.

[2] M. Fathizadeh, H.N. Tien, K. Khivantsev, Z. Song, F. Zhou, M. Yu, Polyamide/nitrogen-doped graphene oxide quantum dots (N-GOQD) thin film nanocomposite reverse osmosis membranes for high flux desalination, Desalination, 451 (2019) 125–132.

[3] M.T. Ravanchi, T. Kaghazchi, A. Kargari, Application of membrane separation processes in petrochemical industry: a review, Desalination, 235 (2009) 199–244.

[4] M.T.M. Pendergast, E.M.V. Hoek, A review of water treatment membrane nanotechnologies, Energy Environ. Sci., 4 (2011) 1946–1971.

[5] B. Lee, Y. Baek, M. Lee, D.H. Jeong, H.H. Lee, J. Yoon, Y.H. Kim, A carbon nanotube wall membrane for water treatment, Nat. Commun., 6 (2015) 7109, doi: 10.1038/ncomms8109.

[6] P. Marchetti, M.F.J. Solomon, G. Szekely, A.G. Livingston, Molecular separation with organic solvent nanofiltration: a critical review, Chem. Rev., 114 (2014) 10735–10806.

[7] M. Elimelech, W.A. Phillip, The future of seawater desalination: energy, technology, and the environment, Science, 333 (2011) 712–717.

[8] M. Fathizadeh, W.L. Xu, F. Zhou, Y. Yoon, M. Yu, Graphene oxide: a novel 2-dimensional material in membrane separation for water purification, Adv. Mater. Interfaces, 4 (2017) 1600918, doi: 10.1002/admi.201600918.

[9] M. Fathizadeh, A. Aroujalian, A. Raisi, Preparation and characterization of thin film composite reverses osmosis membranes with wet and dry support layer, Desal. Water Treat., 56 (2015) 2284–2295.

[10] A. Soroush, J. Barzin, M. Barikani, M. Fathizadeh, Interfacially polymerized polyamide thin film composite membranes: preparation, characterization and performance evaluation, Desalination, 287 (2012) 310–316.

[11] H.A. Shawkya, R. Yaseenb, Y.H. Kotpa, Biosynthesis of silver nanoparticles and its effect on TFC RO membrane for groundwater desalination, Desal. Water Treat., 193 (2020) 34–47.
[12] L. Sidney, S. Srinivasa, D.E. Weaver, High Flow Porous Membranes for Separating Water from Saline Solutions, Google Patents, 1964.
[13] R.J. Petersen, Composite reverse osmosis and nanofiltration membranes, J. Membr. Sci., 83 (1993) 81–150.
[14] K.J. Mysels, W.J.L. Wrasidlo, Strength of interfacial polymerization films, Langmuir, 7 (1991) 3052–3053.
[15] H. Sun, B. Liu, D. Li, J. Yao, Enhancing TFC membrane permeability by incorporating single-layer MSN into polyamide rejection layer, Appl. Surf. Sci., 509 (2020) 145397, doi: 10.1016/j.apsusc.2020.145397.
[16] H.G. Park, Y.D. Jung, S.P. Hong, Effects of interfacial polymerization conditions on performance of polyamide reverse osmosis membranes and optimization of polymerization conditions by statistical methodology, Desal. Water Treat., 74 (2017) 1–11.
[17] Z. Jiang, S. Karan, A.G. Livingston, Water transport through ultrathin polyamide nanofilms used for reverse osmosis, Adv. Mater., 30 (2018) 1705973, doi: 10.1002/adma.201705973.
[18] D.L. Zhao, S. Japip, Y. Zhang, M. Weber, C. Maletzko, T.S. Chung, Emerging thin-film nanocomposite (TFN) membranes for reverse osmosis: a review, Water Res., 173 (2020) 115557–115571.
[19] L. Shen, M. Yi, L. Tian, F. Wang, D. Chun, S. Sun, A. Lu, L. Su, Y. Wang, Efficient surface ionization and metallization of TFC membranes with superior separation performance, antifouling and anti-bacterial properties, J. Membr. Sci., 586 (2019) 84–97.
[20] D. Zhang, Z. Yao, H. Zhang, G. Zhu, L. Liu, C.J.D. Gao, A novel strategy to fabricate thin film nanocomposite reverse osmosis membranes with enhanced desalination performance, Desal. Water Treat., 145 (2019) 70–82.
[21] Y. Li, S. Yang, K. Zhang, B.V.D. Bruggen, Thin film nanocomposite reverse osmosis membrane modified by two dimensional laminar MoS_2 with improved desalination performance and fouling-resistant characteristics, Desalination, 454 (2019) 48–58.
[22] S. Han, Z. Wang, S. Cong, J. Zhu, X. Zhang, Y. Zhang, Root-like polyamide membranes with fast water transport for high-performance nanofiltration, J. Mater. Chem., 8 (2020) 25028–25034.
[23] L. Xu, B. Shan, C. Gao, J. Xu, Multifunctional thin-film nanocomposite membranes comprising covalent organic nanosheets with high crystallinity for efficient reverse osmosis desalination, J. Membr. Sci., 593 (2020) 117398, doi: 10.1016/j.memsci.2019.117398.
[24] Y. Zhang, L. Yang, K.P. Pramoda, W. Gai, S. Zhang, Highly permeable and fouling-resistant hollow fiber membranes for reverse osmosis, Chem. Eng. Sci., 207 (2019) 903–910.
[25] V. Vatanpour, A. Sanadgol, Surface modification of reverse osmosis membranes by grafting of polyamidoamine dendrimer containing graphene oxide nanosheets for desalination improvement, Desalination, 491 (2020) 114442, doi: 10.1016/j.desal.2020.114442.
[26] Y. Zhang, Y. Wan, G. Pan, H. Yan, X. Yao, H. Shi, Y. Tang, X. Wei, Y. Liu, Surface modification of polyamide reverse osmosis membrane with organic-inorganic hybrid material for antifouling, Appl. Surf. Sci., 433 (2017) 139–148.
[27] H.D. Raval, M.D. Samnani, M.V. Gauswami, Surface modification of thin film composite reverse osmosis membrane by glycerol assisted oxidation with sodium hypochlorite, Appl. Surf. Sci., 427 (2018) 37–44.
[28] P. Lu, W. Li, S. Yang, Y. Liu, Q. Wang, Y. Li, Layered double hydroxide-modified thin–film composite membranes with remarkably enhanced chlorine resistance and anti-fouling capacity, Sep. Purif. Technol., 220 (2019) 231–237.
[29] X. Li, Y. Yuan, L. Liu, Y.-S. Leung, Y. Chen, Y. Guo, Y. Chai, 3D printing of hydroxyapatite/tricalcium phosphate scaffold with hierarchical porous structure for bone regeneration, Bio-Des. Manuf., 3 (2020) 15–29.
[30] T. Agarwal, V. Onesto, L. Lamboni, A. Ansari, T.K. Maiti, P. Makvandi, M. Vosough, Engineering biomimetic intestinal topological features in 3D tissue models: retrospects and prospects, Bio-Des. Manuf., 4 (2021) 568–595.
[31] Y. Gong, Z. Bi, X. Bian, A. Ge, J. He, W. Li, H. Shao, G. Chen, X.J.B.-D. Zhang, Study on linear bio-structure print process based on alginate bio-ink in 3D bio-fabrication, Bio-Des. Manuf., 3 (2020) 109–121.
[32] H.B. Park, J. Kamcev, L.M. Robeson, M. Elimelech, B.D. Freeman, Maximizing the right stuff: the trade-off between membrane permeability and selectivity, Science, 356 (2017) 1138–1148.
[33] G.M. Geise, H.-S. Lee, D.J. Miller, B.D. Freeman, J.E. McGrath, D.R. Paul, Water purification by membranes: the role of polymer science, Polym. Sci. B, 48 (2010) 1685–1718.
[34] C. Bellona, J.E. Drewes, P. Xu, G. Amy, Factors affecting the rejection of organic solutes during NF/RO treatment-a literature review, Water Res., 38 (2004) 2795–2809.
[35] M. Zargar, B. Jin, S. Dai, An integrated statistic and systematic approach to study correlation of synthesis condition and desalination performance of thin film composite membranes, Desalination, 394 (2016) 138–147.
[36] Y.-J. Tang, Z.-L. Xu, S.-M. Xue, Y.-M. Wei, H.J. Yang, A chlorine-tolerant nanofiltration membrane prepared by the mixed diamine monomers of PIP and BHTTM, J. Membr. Sci., 498 (2016) 374–384.
[37] Z. Zhang, G. Kang, H. Yu, Y. Jin, Y.J.D. Cao, From reverse osmosis to nanofiltration: precise control of the pore size and charge of polyamide membranes via interfacial polymerization, Desalination, 466 (2019) 16–23.
[38] J. Shi, W. Wu, Y. Xia, Z. Li, W. Li, Confined interfacial polymerization of polyamide-graphene oxide composite membranes for water desalination, Desalination, 441 (2018) 77–86.
[39] S. Lin, H. Huang, Y. Zeng, L. Zhang, L. Hou, Facile surface modification by aldehydes to enhance chlorine resistance of polyamide thin film composite membranes, J. Membr. Sci., 518 (2016) 40–49.
[40] D. Hu, Z.L. Xu, Y.M. Wei, A high performance silica–fluoropolyamide nanofiltration membrane prepared by interfacial polymerization, Sep. Purif. Technol., 110 (2013) 31–38.
[41] H.Z. Zhang, Z.L. Xu, Y.J. Tang, H. Ding, Highly chlorine-tolerant performance of three-channel capillary nanofiltration membrane with inner skin layer, J. Membr. Sci., 527 (2017) 111–120.
[42] Y. Liu, B. Lin, W. Liu, J. Li, C. Gao, Q. Pan, Preparation and characterization of a novel nanofiltration membrane with chlorine-tolerant property and good separation performance, RSC Adv., 8 (2018) 36430–36440.
[43] S. Yu, M. Liu, Z. Lu, Y. Zhou, C. Gao, Aromatic-cycloaliphatic polyamide thin-film composite membrane with improved chlorine resistance prepared from m-phenylenediamine-4-methyl and cyclohexane-1,3,5-tricarbonyl chloride, J. Membr. Sci., 344 (2009) 155–164.
[44] B.C. Donose, S. Sukumar, M. Pidou, Y. Poussade, J. Keller, W. Gernjak, Effect of pH on the ageing of reverse osmosis membranes upon exposure to hypochlorite, Desalination, 309 (2013) 97–105.
[45] S. Bing, J. Wang, H. Xu, Y. Zhao, Y. Zhou, L. Zhang, C. Gao, L. Hou, Polyamide thin-film composite membrane modified with persulfate for improvement of perm-selectivity and chlorine-resistance, J. Membr. Sci., 555 (2018) 318–326.
[46] V.T. Do, C.Y. Tang, M. Reinhard, J.O. Leckie, Degradation of polyamide nanofiltration and reverse osmosis membranes by hypochlorite, Environ. Sci. Technol., 46 (2012) 852–859.
[47] Y.-J. Tang, Z.-L. Xu, S.-M. Xue, Y.-M. Wei, H. Yang, Improving the chlorine-tolerant ability of polypiperazine-amide nanofiltration membrane by adding NH_2-PEG-NH_2 in the aqueous phase, J. Membr. Sci., 538 (2017) 9–17.
[48] Z. Zhang, G. Kang, H. Yu, Y. Jin, Y. Cao, Fabrication of a highly permeable composite nanofiltration membrane via interfacial polymerization by adding a novel acyl chloride monomer with an anhydride group, J. Membr. Sci., 570–571 (2019) 403–409.
[49] Z.-Y. Ma, X. Zhang, C. Liu, S.-N. Dong, J. Yang, G.-P. Wu, Z.-K. Xu, Polyamide nanofilms synthesized via controlled interfacial

polymerization on a "jelly" surface, Chem. Commun., 56 (2020) 7249–7252.
[50] H.W. Peng, W.-H. Zhang, W.-S Hung, N.X. Wang, J. Sun, K.-R. Lee, Q.F. An, C.-M. Liu, Q. Zhao, Phosphonium modification leads to ultrapermeable antibacterial polyamide composite membranes with unreduced thickness, Adv. Mater., 32 (2020) 2001383, doi: 10.1002/adma.202001383.
[51] J.V. Nicolini, C.P. Borges, H.C. Ferraz, Selective rejection of ions and correlation with surface properties of nanofiltration membranes, Sep. Purif. Technol., 171 (2016) 238–247.
[52] H. Li, W. Shi, Y. Zhang, Q. Du, X. Qin, Y. Su, Improved performance of poly(piperazine amide) composite nanofiltration membranes by adding aluminum hydroxide nanospheres, Sep. Purif. Technol., 166 (2016) 240–251.
[53] S. Avlonitis, W.T. Hanbury, T. Hodgkiess, Chlorine degradation of aromatic polyamides, Desalination, 85 (1992) 321–334.

Supplementary information

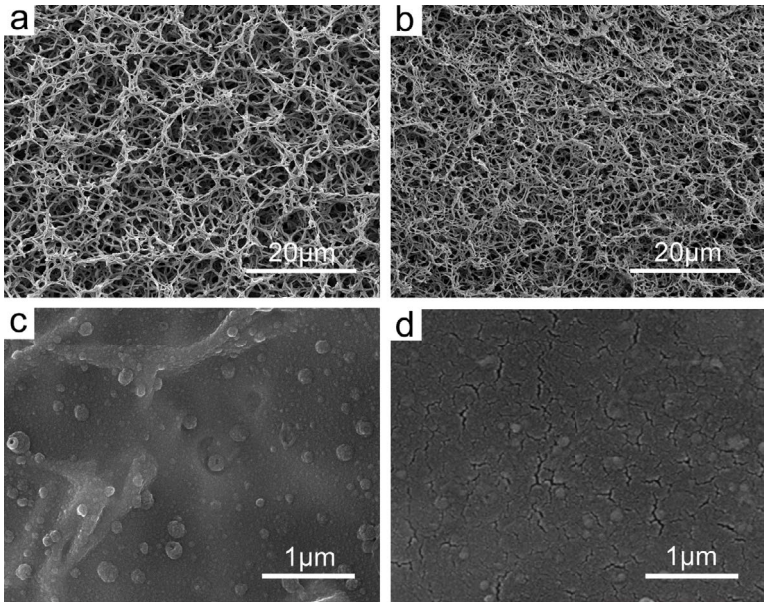

Fig. S1. SEM images of (a) front surface and (b) back surface of PA66 support layer; SEM images of (c) FI-IP membranes prepared with m-XDA and TMC concentrations of 0.3–0.15 wt.%; SEM images of (d) BLFIP1 membranes.

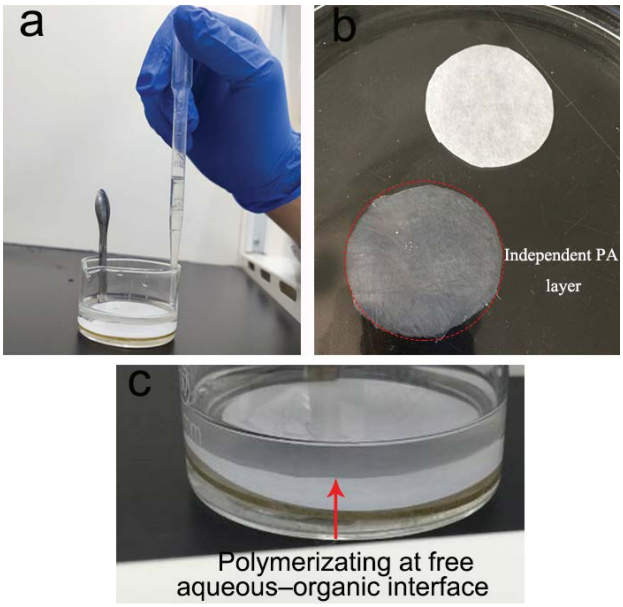

Fig. S2. (a) Optical images of the TMC dropped slowly onto the surface of the buffer layer and (b) optical images of obtaining a independent PA layer; Optical images of interfacial (c) polymerization of PA at a free aqueous–organic interface.

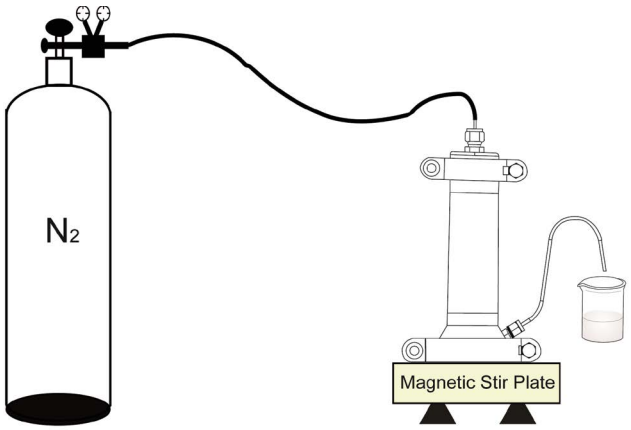

Fig. S3. Process flow chart of desalting test.

Table S1
The percentage for the chemical species of the peak split of C1s measured from surface of the BLFIP membranes

C1s	Percentage of each peak			
	C–C (%)	C–N (%)	N–C=O (%)	O–C=O (%)
BLFIP1	66.05	24.16	6.15	3.64
BLFIP2	64.55	25.65	6.18	3.62
BLFIP3	63.02	27.01	6.22	3.57
BLFIP4	61.05	29.19	6.21	3.55
BLFIP5	58.09	32.18	6.18	3.55

Table S3
Rejections of BLFIP and m-XDA/TMC based PA membrane prepared by IP

Pressure (bar)	R_{HIn} (%)	$R_{Na_2SO_4}$ (%)	R_{MgSO_4} (%)	R_{NaCl} (%)	References
10.0	–	94.6	54.5	36.2	[S3]
5.0	95.16	92.55	92.01	83.99	This work

Table S2
Salt rejection of different membranes

Operating pressure (bar)	Rejection for HIn (%)	Rejection for Na_2SO_4 (%)	Rejection for $MgSO_4$ (%)	Rejection for NaCl (%)	References
4.0	–	97.7	90.5	15.1	[S1]
6.0	–	98.4	93.8	22.1	[S2]
5.0	95.16	92.55	92.01	83.99	This work

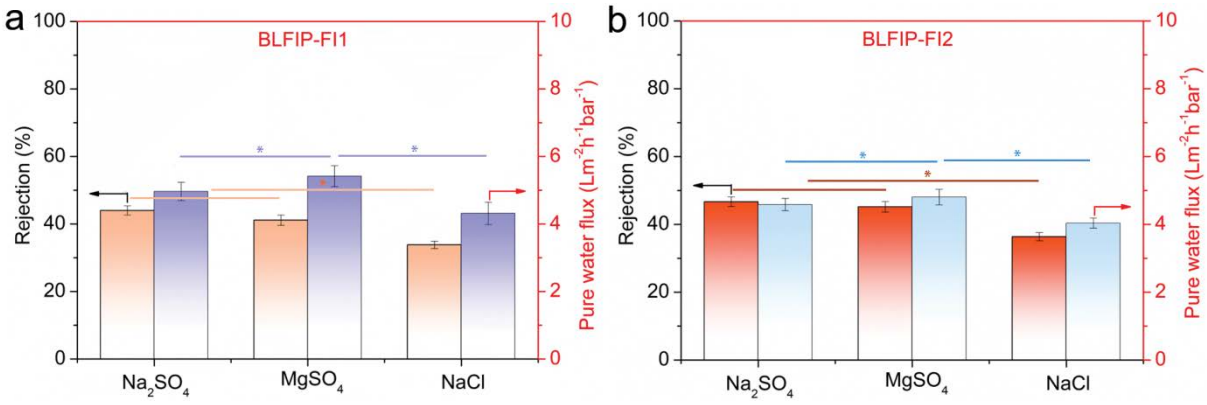

Fig. S4. The salt rejection and water flux of (a) FIP-FI1 and (b) FIP-FI2 membranes.

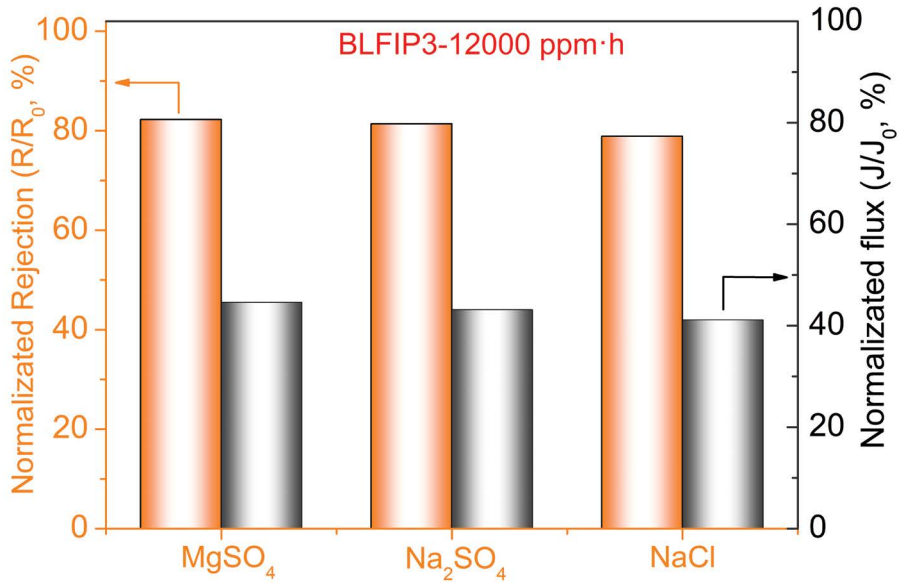

Fig. S5. Chlorine-resistant performance of BLFIP3 (It was prepared with m-XDA and TMC concentrations of 0.5–0.25 wt.%).

References

[S1] Z.-Y. Ma, X. Zhang, C. Liu, S.-N. Dong, J. Yang, G.-P. Wu, Z.-K. Xu, Polyamide nanofilms synthesized via controlled interfacial polymerization on a "jelly" surface, Chem. Commun., 56 (2020) 7249–7252.

[S2] H.W. Peng, W.-H. Zhang, W.-S Hung, N.X. Wang, J. Sun, K.-R. Lee, Q.F. An, C.-M. Liu, Q. Zhao, Phosphonium Modification Leads To Ultrapermeable Antibacterial Polyamide Composite Membranes With Unreduced Thickness, Adv. Mater., 32 (2020) 2001383–2001389.

[S3] Y. Liu, B. Lin, W. Liu, J. Li, C. Gao, Q. Pan, Preparation and characterization of a novel nanofiltration membrane with chlorine-tolerant property and good separation performance, RSC Adv., 8 (2018) 36430–36440.